(Article begins on next page)

Solar and interplanetary triggers of the largest *Dst* variations of solar cycle 23

Y. Cerrato[1], E. Saiz[1], C. Cid[1], W. D. Gonzalez[2] and J. Palacios[3]

[1]Space Research Group - Space Weather, Departamento de Física, Universidad de Alcalá, Spain

[2]Instituto Nacional de Pesquisas Espaciais, Brazil

[3]Image Processing Laboratory, Universidad de Valencia, Spain

Abstract. We present the results of an investigation from the Sun to the Earth of the sequence of events that caused major *Dst* decreases ($\Delta Dst \leq$ -100 nT during one hour) that occurred during 1996–2005. These events are expected to be better related to GIC (geomagnetic induced currents) events, than those events where any geomagnetic index is far from its quiet time value. At least one full halo CME with a speed on the plane of sky above 900 km/s participates in every studied event. The seven events were triggered by interplanetary signatures which arise as a consequence of interaction among different solar ejections. The interaction arises at different stages from the solar surface, between segments of a filament, to the interplanetary medium, appearing as ejecta or MultiMCs (multiple-magnetic cloud). In other cases, shock waves overtake or compress previous ICMEs and at other times the interaction appears also between MCs (magnetic clouds) and streams.

1. Introduction

As solar wind disturbances from solar ejections interact with the Earth's magnetic field, large electric currents arise in the terrestrial magnetosphere, ionosphere and in the conducting ground. As a consequence, geomagnetic induced currents (GIC) also arise in technological systems, leading to failures in the normal operation of the systems. Large number of studies has been devoted to the understanding of the solar and interplanetary sources of these geomagnetic events [e.g. Gonzalez et al., 1999; Burlaga et al., 2001; Cid et al., 2004; Huttunen et al., 2005; Gonzalez et al., 2007; Zhang et al., 2007; Echer et al., 2008a,b; Lario et al., 2008].

Different geomagnetic indices, such as *Dst*, *AE*, or *PC* indices, have been established to quantify the geomagnetic disturbance at different latitudes at the terrestrial surface. Other indices, such as *Kp* or *am*, have been considered as proxies of

44 the planetary disturbance. However, the *Dst* index has been used extensively as the

45 proxy for the intensity of the overall disturbance [Gonzalez et al., 1994]. Choosing the

46 minimum value reached by the *Dst* index, or Dst_{peak}, as a proxy for the severity of the

47 storm, some failures in technological systems could pass as not related to space weather,

48 even if they were. As an example, we can cite the papers by Belov et al. [2007] and

49 Eroshenko et al. [2010] about the relationship between the response of the

50 Signalization, Centralization and Blockage (SCB) system in the high-latitude parts of

51 Russian railways and severe geomagnetic storms. In Table 1 of Eroshenko et al. [2010]

52 a list of magnetic storms appears where failures occurred in the automatic railway

53 system SCB. For most of these events, the *Dst* index peaked below -200 nT or even

54 below -400 nT, but failures were also registered on January 21, 2005 when *Dst* reached

55 only -105 nT, or on April 8, 2001, when *Dst* just reached -51 nT.

56 Koen and Gaunt [2002] conclude that the *K*-index and NOAA classification of

57 storm severity are not directly related to the magnitude of GICs in networks. They

58 suggest that an improved index for representing the severity of storms and, ideally,

59 issuing warnings, should include the magnitude of the magnetic field variation with

60 time, which determines the electric field available to drive GICs. Therefore, choosing

61 the value for the maximum disturbance as measured by other indices instead of Dst_{peak}

62 does not solve the problem. On this line Vodyannikov et al. [2006] conclude that

63 unwanted consequences could arise in power systems during long periods with the time

64 derivative of the geomagnetic field horizontal component exceeding 30 nT/min.

65 Therefore, the reason for the failures related to GICs should be analyzed, not only

66 looking how much the terrestrial magnetic field varies but also looking how fast it

67 changes.

68   In this scenario, the aim of this paper is to address the solar and interplanetary

69   sources of the largest variations of the *Dst* index along the last solar cycle. The

70   understanding of the triggers of large decreases in *Dst* can be also considered an

71   advance related to the fact that we are dealing with the largest way of disturbance of the

72   terrestrial magnetosphere. In Section 2 we set the criterion to select the events to be

73   studied and in Section 3 we carry out a detailed analysis about the interplanetary causes

74   and also provide an identification of solar sources which that could have triggered the

75   events. Finally, our conclusions are given in Section 4.

76   **2. Events selection**

77   As previously pointed out by Koen and Gaunt [2002], GIC events are related to

78   the magnitude of the magnetic field intensity variation with time at the terrestrial

79   surface. Previous studies computed the time derivative of the magnetic field horizontal

80   component (*dH/dt*) using the highest resolution data available from local

81   magnetometers. However, there is not any systematic study about the resolution of

82   magnetic field data that should be used in order to calculate *dH/dt* for purposes of space

83   weather forecasting.

84   Figures 6 to 9 of Eroshenko et al. [2010] show *Kp* and *Dst* indices for the

85   geomagnetically disturbed periods analyzed in the paper, together with the times of the

86   observed anomalies. Just at first glance of those Figures one can observe that *Dst*

87   (which is an hourly index) showed fast drops at that time. Specifically, all failures in

88   the SCB system, from Table 1 of Eroshenko et al. [2010], took place when the time

89   derivative of *Dst* calculated as $Dst_{t+1hour}$ - Dst_t, was below -50 nT/hour.

90   There were 31 events where $dDst/dt \leq$ -50 nT/hour during solar cycle 23 [Saiz et

91   al., 2008]. This number of events is too large to perform a detailed study of the solar

92 and interplanetary drivers which were related to the large time derivative of *Dst* and

93 therefore to the probability of a GIC event. Therefore, we are undertaking this study by

94 choosing a threshold of *dDst/dt* = -100 nT/hour, thus reducing in this way the number of

95 events to be carefully analyzed. Based on this criterion, we analyze seven events which

96 are listed in Table 1. This table shows event number, the date (year, month, day, hour)

97 where the minimum hourly variation $(dDst/dt)_{min}$ takes place, the corresponding Dst_{peak}

98 value and the associated interplanetary candidate for the large *Dst* variation.

99   Five out of the seven analyzed events are superstoms, with peak *Dst* reaching

100 less than -250 nT [Echer et al. 2008a]. The peak *Dst* index for the other two events were

101 below -200 nT. Therefore, all of them have been previously analyzed in the literature

102 [e.g. Echer et al., 2008a; Cid et al., 2008; Gopalswamy, 2007; Zhang et al., 2007, Xie et

103 al. 2006, Wang, 2007]. However, the aim of this work is to highlight the common

104 features that may have triggered the largest hourly variation of the *Dst* index.

105   Throughout this paper, we review the literature related to the seven selected

106 events, paying special attention to the possible solar and interplanetary events related to

107 the large and sharp decrease of the *Dst* index. For that task we use the LASCO CME list

108 (http://lasco-www.nrl.navy.mil/cmelist.html), the Hα and X-ray flare events from the

109 National   Geophysical   Data   Center   (http://www.ngdc.noaa.gov/stp/

110 SOLAR/flareint.html), and the solar wind magnetic field and plasma data shifted to the

111 Earth's Bow Shock Nose from OMNIweb database (http://omniweb.gsfc.nasa.gov/

112 ow_min.html) with one minute resolution. The seven events are described in order of

113 decreasing absolute value of the *dDst/dt* in the following Section.

3. Description of the solar and interplanetary triggers of the events

3.1 Event on May 15, 2005

116   The first event of Table 1 gives the impression of an event which can be easy

117   followed throughout the whole Sun-Earth chain: an M8.0 flare on May 13, 2005 at

118   16:13 UT related to the eruption of the large sigmoidal structure in NOAA active region

119   10759, which released the CME observed by LASCO at 17:22 UT. Then, in-situ

120   measurements at L_1 (ACE), Figure 1, show low temperature, high magnetic field

121   strength and a smooth rotation through a large angle of the magnetic field vector, which

122   are common features of a magnetic cloud (MC) [Burlaga et al., 1981], the interplanetary

123   counterpart of a subset of CMEs. A few hours later, a geomagnetic disturbance appears

124   at the terrestrial environment. These almost 'academic' features along the solar-

125   terrestrial chain have been assumed as the scenario of this event [e.g. Yurchyshyn et al.,

126   2006, Zhang et al., 2007]. However, there are three facts which guide Dasso et al.

127   [2009] to consider a different scenario: (1) the too high magnetic field strength (higher

128   than 50 nT), far from typical values for magnetic clouds at 1AU, which have enhanced

129   magnetic field strength in the range of 15-30 nT [Lepping et al., 1990]; (2) the

130   problems trying to reproduce the magnetic topology with a single magnetic flux rope,

131   and (3) the long duration of the cloud as it passes the spacecraft (1 day and 9 hours,

132   considering the boundaries identified by Yurchyshyn et al. [2006] or 16.6 hours as

133   identified at http://wind.nasa.gov/mfi/mag_cloud_pub1.html). This long travel time

134   crossing the ACE spacecraft, together with the large velocity (almost 1000 km/s), led

135   these authors to estimate a diameter of 0.8 or 0.5 AU, respectively, which are far from

136   the common values expected at 1 AU in the range of 0.2-0.4 AU [Lepping et al., 1990].

137   The detailed study made by Dasso et al. [2009] provides strong arguments to

138   consider that there are two different eruptions coming from different parts of the same

139   filament, which interact at some place in the interplanetary medium before reaching L_1

140   point, where they were observed as two attached, but non-merged, magnetic clouds

141 (shadowed areas in Figure 1). Based on type II radio burst features in the kilometer

142 domain, observed by the TNR experiment on WAVES, Dasso et al. [2009] proposed

143 that two solar ejections occurred on May 13, 2005 with a difference of about 4 hours,

144 both from AR 10759, and with the last ejection traveling faster than the first one (almost

145 twice) and interacting at some place between the Sun and the Earth. As a result, a

146 compression of the first magnetic cloud by the second one might be related to the large

147 magnetic field B_z component, which passes from +37 nT to -44 nT in less than 40

148 minutes (staying below -10 nT for more than 3 hours [Gonzalez and Tsurutani, 1987]),

149 with the corresponding enhancement of the geoeffectiveness at the terrestrial

150 environment. On May 15 (doy 135) *dDst/dt* was less than -100 nT/hour in two

151 successive intervals: between 05 UT and 06 UT (from +30 nT to -77 nT) and between

152 06 UT and 07 UT (from -77 nT to -247 nT). The large decrease of *Dst* (277 nT between

153 05 to 07 UT) could be related to the small magnetic cloud described by Dasso et al.

154 [2009] and the preceding sheath, which is compressed by the second one resulting in a

155 larger magnetic field strength [Wang et al, 2005; Lugaz et al, 2005].

156 **3.2 Event on November 6, 2001**

157 Solar wind measurements show a complex magnetic structure for the second

158 event of Table 1, November 6, 2001 (Figure 2). An overlapping shock on November 6

159 (doy 310) at 01:24 UT (dashed line and "S" in Figure 2) is a clear indicator of

160 interaction among several solar ejections [Wang et al., 2003a]. The compression

161 between this shock and the preceding magnetic cloud (see front boundary indicated by a

162 dashed-dotted line in Figure 2) increased the geoeffectiveness triggering the large

163 decrease of *Dst* index from -101 nT on November 6 (doy 310) at 02 UT to -269 nT at 03

164 UT. Although the Sun was very active on that date, Xie et al. [2006] stated that three

165 full halo CMEs were the solar sources related to this disturbance. They also stated that

166   the event involved a high speed stream. The onset of the first CME at LASCO C2

167   coronagraph was November 1 at 22:30 UT, whose velocity in the plane of the sky was

168   453 km/s. An M1.1 flare related to this CME started at GOES at 21:38 UT in N12W23

169   (active region NOAA 9682). The second CME was observed by LASCO C2 on

170   November 3 at 19:20 UT with a linear fit speed of 457 km/s and related to case an X-

171   class flare from N06W18 (active region NOAA 9684). Finally another full halo was

172   seen by LASCO on November 4 at 16:35 UT associated to an M2.1 class flare from the

173   active region NOAA 9684, as the previous CME, but with a speed of 1810 km/s, about

174   four times the speed of the previous CMEs. As a result, the two first front halo CMEs,

175   from different active regions, but very close in the solar surface, are expected to interact

176   with the last one, increasing in an extraordinary way the magnetic field B_z component

177   until -77 nT, staying below -40 nT for more than two hours. After that, a large

178   disturbance took place at terrestrial environment as indicated by *Dst* index, that peaked -

179   292 nT after a two-steps main phase [Cid et al., 2008]. Although the number of peaks in

180   *Dst* is not necessarily directly related to the number of interplanetary transients that are

181   involved in generating the storm [Richardson and Zhang, 2008], Farrugia et al. [2006]

182   proposed that interacting ejecta are an important interplanetary source of double-dip

183   major storms. Specifically for this event, the main phase starts with the arrival of the

184   magnetic cloud . Then, the second dip in *Dst* index, where *Dst* decreases -168 nT in one

185   hour, corresponds to the arrival of the overtaking shock on November, 6 (doy 310) at

186   01:24 UT. The time of the shock arrival corresponds to the shock time at magnetic field

187   data, as there is a large data gap at solar wind data both, at Ace and Wind spacecraft.

188   Although this data gap does not provide quantitative density values, they should be

189   large enough to saturate solar wind plasma instruments on board and, as a consequence,

190   to produce a large dip, as proposed by Farrugia et al. [2006] for the event on March 31,

191   2001. In that event, the major factor determining the intensity of the storm was the very

192   high plasma sheet density, well correlated with the very high solar wind density.

193   Therefore, we can conclude that this overtaking shock, which was also identified by

194   Zhang et al. [2007a, b] as an ICME driven shock propagating through a preceding

195   ICME, was the cause of the large $dDst/dt$ for this event.

196   **3.3 Event on August 24, 2005**

197   Figure 3 shows interplanetary data and Dst index measured for the period

198   August 23-25, 2005 (doys 235-237) that corresponds to the third event of Table 1. At a

199   first glance the geomagnetic storm seems to be associated with a corotating interaction

200   region (CIR) created by a fast wind interacting with a previous slow wind (see fifth

201   panel in Figure 3). As expected, the region between both winds exhibits a high

202   temperature and a highly fluctuating B_z component. Looking at EIT images (Figure 4), a

203   coronal hole appears clearly at the solar surface close to the disk center where the fast

204   stream emanates from. However, this kind of interplanetary events usually is related to

205   moderate storms where -50 nT $> Dst >$ -100 nT [Xu et al., 2009, Gonzalez et al., 1999],

206   and the main phases of the resultant magnetic storms typically have irregular profiles.

207   As a result, large hourly variations in Dst are not expected for such interplanetary

208   signatures, but small decreases one after another. However, in this case, the Dst index

209   decreases from -22 nT on August 24 (doy 236) at 09 UT to -180 nT at 10 UT

210   (shadowed area on bottom panel of Figure 3). This large variation in Dst is associated

211   with a one hour interval where B_z reaches values below -50 nT, which is not usual

212   inside a CIR, for which field strengths fall typically in the range of 5 to 15 nT at 1 AU

213   [Zhang et al., 2008]. This high magnetic field strength corresponds to a region where B_z

214   can be considered smooth, and the temperature is relatively low. These signatures

215   indicate that the spacecraft is inside an interplanetary coronal mass ejection (ICME),

216 which drives the forward shock on August 24 (doy 236) at 06:10 UT (dashed line and

217 "S" in Figure 3). Moreover, the clear rotation of the B_x and B_y magnetic field

218 components along with B_z maximum when both x and y components get zero value,

219 indicates that it presents a flux rope structure with its axis pointing along the z axis

220 (shadowed area in top panels).

221 About the solar source of this magnetic cloud, two different M-class flares took

222 place on August 22, 2005 both of them from the active region NOAA 10798. The first

223 one (M2.6), starting at 00:44 UT from S11W54, was related to the CME described

224 above, with a speed of 1194 km/s, and a second one, more intense (M5.6), at 16:46 UT

225 from S13W65 and related to a CME with onset at LASCO C2 at 17:30 UT and with a

226 speed of 2378 km/s. Both of them have been related to this geomagnetic storm by

227 Zhang et al. [2007]. However, only one ICME is observed at L1. The assignment of the

228 correct CME to the signatures observed at L1 is out of the scope of this study.

229 As stated above, the sharp decrease on *Dst* was related to the sharp increase in

230 the B_z component and therefore, the question to be addressed is what produced such a

231 high magnetic field strength inside the ICME. A careful analysis of solar wind data for

232 the whole event is necessary for this task. Solar wind density remains above 30 cm^{-3}

233 after the shock until the ICME passage when it decreases sharply until around 10 cm^{-3}

234 and then starts a new increase until around 40 cm^{-3}. Then, between 11:39 and 12:00 UT,

235 the density drops to about 20 cm^{-3} and the temperature increases suddenly from below

236 5×10^6 K to above 10^7 K. This region corresponds to the stream interface which separates

237 slow and fast solar wind streams [Burlaga, 1974; Gosling et al., 1978].

238 An inspection of a time sequence of SOHO EIT 28.4 nm images (Figure 4)

239 reveals that after the ejection of a halo CME on August 22 at 01:31 UT, the size of a

240 coronal hole close to the central solar meridian increased towards the West, indicating

241 an interaction between the active region NOAA 10798 and the coronal hole mentioned

242 above, which can be guessed from in-situ measurements. As stated above, solar wind

243 temperature and density values increased before the arrival of the stream interface

244 suggesting that the magnetic cloud was compressed by the fast stream. As the coronal

245 hole is close to the solar equator and the magnetic cloud axis follows the z direction, the

246 magnetic cloud is expected to be carried away from the Sun by the stream as a small-

247 scale transient caught in the compression region between the two streams, as shown by

248 Rouillard et al. [2009]. This kind of interaction between active regions, involving flares

249 and/or filament eruptions, occurring close to growing low-latitude coronal holes was

250 already associated with intense geomagnetic activity by Gonzalez et al. [1996].

251 **3.4 Event on March 31, 2001**

252 Wang et al [2003b, 2005] proposed and simulated a structure named multiple-

253 magnetic cloud (Multi-MC) for the signatures observed in the solar wind of the event on

254 March 31, 2001 (number 4 of Table 1). In contrast to complex ejecta, a Multi-MC is

255 formed by a series of successive MCs (or sub-clouds), which satisfy the criteria of a

256 typical magnetic cloud, and interacting regions between them. In this event, two clouds

257 can be easily distinguished in the solar wind data (shadowed regions in Figure 5),

258 separated by an increase in plasma beta [Wang et al., 2003b]. Other ejecta complete the

259 in-situ events. The sub-clouds and ejecta observed in the solar wind are the counterparts

260 of three full halo CMEs on March 28 at 01:27 UT, 12:50 UT and March 29 at 10:26 UT

261 from NOAA 9393, when the active region was passing through the solar central

262 meridian. The increasing velocity of the three CMEs (427 km/s, 519 km/s and 942 km/s

263 respectively) let the latter to reach the former ones, with a consequent compression of

264 the magnetic field lines, leading to B_z values of about -50 nT and therefore enhancing

265   their geoeffectiveness. Thus *Dst* decreased from -8 nT on March 31 (doy 90) at 04 UT

266   to -156 nT at 05 UT and to -256 nT at 06 UT, decreasing twice the threshold -100

267   nT/hour. Both decreases are related to the highly fluctuating southern B_z in the sheath

268   field and the interface before the long and large southern B_z of the first sub-cloud.

269   **3.5 Event on July 15, 2000**

270   The event number five of Table 1, also known as the Bastille Day event, has

271   been widely studied by several authors [see as an example a monograph of *Solar*

272   *Physics* (Volume 204, Issue 1/2, 2001) devoted to this event]. The full halo CME on

273   July 14, 2000 at 10:54 UT on LASCO C2 coronagraph was associated with a flare

274   observed by EIT from AR9077 at N16.8E0.21 at 10:12UT and with an X5.7 class flare

275   event reported by GOES from this same area starting at 10:03 UT. The solar event and

276   its interplanetary counterpart have been extensively analyzed, but a question should still

277   be solved: what is the cause of the very large interplanetary magnetic field B_z

278   component, which reached -60 nT and kept below -30 nT for more than 1.5 hours,

279   making *Dst* to drop from -61 nT on July 15 (doy 197) at 19 UT to -198 nT at 20 UT?

280   Could it be related to the high velocity of the CME [Gonzalez et al. 1998]? Of course

281   this could be an answer, however, a careful inspection of this event reveals similar

282   features to those described above which could indicate interaction between different

283   solar ejections from the same active region. Several M and X class flares were reported

284   by GOES between July 10 to 14. The three X class flares were related to full or partial

285   halo CMEs on July 11 at 13:27 UT, on July 12 at 11:06 UT and finally on July 14 at

286   10:54 UT, already mentioned above (other non-halo CMEs were also observed by

287   LASCO for this period and this active region). The linear fit speed provides for these

288   CMEs the values of 1078, 1124 and 1674 km/s, respectively. Several interplanetary

289   shocks were observed during days 11-15 of July in advance of ICMEs. In total, three

290 shocks driven by three ICMEs were observed by Ace within the four-day interval (doys

291 195 to 198) surrounding the Bastille Day event [Smith et al., 2001] (see Figure 6 where

292 the shocks are shown by dashed lines). After the last of the three shocks (doy 197 at

293 14:35 UT at OMNIweb data) the temperature increased extraordinarily until 3×10^6 K

294 and the solar wind density increased to approximately 30 cm^{-3} at 15:03 UT. Then, after

295 about 20 minutes the density values decreased to about 2 cm^{-3} for almost one hour and

296 increased again to above 20 cm^{-3} at 19:06 UT. The last peak in density corresponds to

297 the large drop in Dst and to a highly compressed magnetic field pointing to the south of

298 the ecliptic plane at the rear of the sheath and the beginning of the ICME. These solar

299 wind features fit well with numerical simulations undertaken by Lugaz et al. [2005]

300 where two shocks from two identical CMEs launched in the same direction (the second

301 one 10 hours after the first one) merge and a stronger, faster shock appears where the

302 "new" downstream region is hotter. Therefore, the merging of shock waves may have

303 caused a very strong shock in front of the leading ejecta with a compressed magnetic

304 field in the sheath, leading to southern B_z with extreme values. Nevertheless, as shown

305 in Figure 6, three shocks followed by three ICMEs (corresponding to the three halo

306 CMEs) are observable at 1 AU pointing no merging. Therefore, we cannot be

307 conclusive about the cause for the extraordinarily increased temperature and density and

308 the highly compressed magnetic field observed at solar wind, which could arise as a

309 consequence of successive, but non-merged, shock waves. Numerical simulation could

310 help to get light on this point, although the enhanced temperature ahead the third shock

311 (S3) already indicates that interaction between this shock and the ICME driving the

312 second shock (S2) exists. This interaction might lead to southern B_z with extreme values

313 because of successive shock waves, as previously indicated for merging shock waves.

314   This large B_z, field together with a high solar wind velocity (above 1000 km/s) probably

315   caused the large depression in the *Dst* index (shadowed area in the bottom panel).

3.6 Event on September 17, 2000

317   Several full and partial halo CMEs from the same active region are also related

318   to the event number 6 (September 17, 2000) of Table 1. Two partial halo CMEs on

319   September 15 at 12:06 UT and 15:26 UT and two full halo CMEs on September 15 at

320   21:50 UT and on September 16 at 05:18 UT, all of them related to M class flares from

321   NOAA 9165 active region, have been associated with this geomagnetic storm [Zhang et

322   al., 2007, Burlaga et al., 2001, Xie et al., 2006]. As in the previous case the projected

323   speed of the last CME, 1215 km/s was much larger than the previous ones, with speeds

324   of 633 km/s, 481 km/s and 257 km/s respectively. Then, this CME could have overtaken

325   the former ones as it traveled far away from solar surface developing a complex ejecta

326   [Burlaga et al., 2001, 2002. This was observed at in-situ data (shadowed areas in Figure

327   7), where at least a sub-cloud and an ejecta can be distinguished. The highly fluctuating

328   magnetic field and solar wind velocity on September 18 (doy 262) could also indicate

329   the interaction of these ejections with material coming from the large coronal holes

330   close to the central solar meridian and next to the active region related to the CMEs.

331   The large hourly *Dst* variation took place between 21 UT and 22 UT on September 17

332   (doy 261), when *Dst* dropped from -61 nT to -171 nT. This decrease in *Dst* can be

333   related to several signatures in solar wind inside the sheath of the complex ejecta: 1) a

334   southern B_z, which reached -37 nT and got values below -10 nT for about 2.5 hours, 2) a

335   large increase in solar wind density until above 50 cm^{-3}, and 3) an enhancement in

336   temperature over 10^6 K. The arrival of large $B_z < 0$ interval (1st signature), together with

337   a high solar wind velocity, could have intensified the ring current. Following Farrugia et

338   al. [2006], we consider that the compression of plasma, as deduced from the

339 enhancement in density and temperature in the sheath, could have also played a key role

340 in the *Dst* drop.

3.7 Event on November 20, 2003

342   The seventh and last event from Table 1 (November 20, 2003) presents an

343 interval (wider dashed area in Figure 8) with smooth B_z rotation, enhanced magnetic

344 field strength and relative low temperature, together with a slow decreasing solar wind

345 velocity, which correspond to features of a magnetic cloud. Gopalswamy et al. [2005]

346 has discussed in detail the solar ejection which could be related to this geomagnetic

347 storm, which was the largest of cycle 23. They associated the November 20 magnetic

348 cloud with the 08:50 UT halo CME (speed in the plane of the sky ~1660 km/s) on

349 November 18 from AR501 at S01E33. However, as stated above for other events as the

350 Bastille one, it is not common for the magnetic field strength in magnetic clouds to

351 reach more than 50 nT. Gopalswamy et al. [2005] propose that the extreme field

352 strength of the MC may be due to a combination of two factors: the flux rope originated

353 in an active region instead in a quiescent filament region, and the difference between the

354 MC speed and the upstream speed was relatively large and therefore the MC suffered a

355 strong front-side compression. However, the large *Dst* drop, which takes place on

356 November 20 (doy 324) between 16 UT and 17 UT from -229 nT to -329 nT, cannot be

357 the result of the leading shock (dashed line in Figure 8) or even the sheath before the

358 MC. During the passage of these solar wind features, and also during the first part of the

359 MC passage, *Dst* decreases more or less smoothly (up to 60 per hour), at the same rate

360 as B_z is more and more southern. However, the largest decrease in *Dst* (100 nT in one

361 hour), showed as the narrower dashed area in Figure 8, takes place when southern B_z is

362 increasing and therefore it cannot be related to the extreme field strength of the MC or

363 to the interplanetary shock produced by the difference between the MC speed and the

364 upstream speed.

365   Gopalswamy et al. [2005] suggest also two additional possibilities: the

366 interaction between the high speed stream of the coronal hole, which might compress

367 the MC, and the interaction with another CME from the same region at 08:06 UT (speed

368 in the plane of the sky ~1223 km/s, width ~ 104º). After a careful revision of the event

369 looking at EIT images, we cannot appreciate any change in the size of the coronal hole

370 close to AR501 on November 18, although there are noticeable changes in the size of

371 the coronal hole the day before related to a previous partial halo CME which appears on

372 LASCO C2 field of view on November 17 at 09:26 UT. About the interaction with a

373 previous CME, that possibility should be kept on mind in the analysis of solar wind

374 data, but we think that the MC seen at 1 AU is only related to the CME observed at

375 08:50 UT related to the M3.9 flare at 08:30. In order to explain the previous statement,

376 it is necessary to combine solar observations and solar wind data keeping in mind that

377 the flux rope magnetic structure observed in situ must agree on the sign of the magnetic

378 helicity of the solar region from which it originates. As Gopalswamy et al. [2005] state,

379 the ACE data show that the magnetic field in the MC rotates smoothly with an east-

380 south-west chirality. Yurchyshyn et al. [2005] estimated the AR501 helicity as positive,

381 in agreement with that of the MC. However, Möstl et al. [2008] discussed that

382 concluding that the handedness (or helicity sign) of the very extended filament was

383 ambiguous. Chandra et al. [2009] conclude that the large scale magnetic field of the

384 AR501 has a negative sign, contradicting what is expected from magnetic helicity

385 conservation. However, Chandra et al. [2009] also show the existence of a localized flux

386 of positive helicity in the southern part of AR501 and conclude that during the M3.9/2N

387 flare at 08:30 UT (associated with the halo CME related to the MC) two segments of the

388 filament with opposite chilarities interacted through magnetic reconnection and the

389 helicity carried by both segments partially cancelled, transporting away a net-positive

390 helicity, as measured by ACE at 1 AU.

391   The fact that the interaction between the flux ropes took place at the Sun instead

392 at the interplanetary medium could explain the smooth rotation of the magnetic field, far

393 away from the ejecta or Multi-MC features. However, there are some remaining

394 signatures of this interaction such as the unusual high solar wind density (above

395 20 cm^{-3}) observed in the magnetic cloud (starting at double dashed area). Specifically,

396 proton density increased on November 20 (doy 324) from approximately 5 cm^{-3} to more

397 than 20 cm^{-3} in less than ten minutes (from 16:12 UT to 16:20 UT), although this

398 increase is not too high when compared with the value at the preceding shock and

399 sheath (corresponding to a MC). The temperature is also enhanced by a factor larger

400 than 2 (from below 5×10^4 K before 15:31 UT of doy 324 to above 10^5 K after 15:43 UT)

401 being even higher than solar wind temperature before the forward shock.

402   Farrugia et al. [2006], using a kinetic model to simulate the temporal behavior of

403 the ring current buildup during the passage of an ejecta merger show that the strength of

404 the ring current depends essentially on two factors: the convection electric field in

405 which particles drift, and the seed density population. Using as a case the two-step

406 storm on March 31, 2001, they show that the hot dense plasma sheet was of solar origin,

407 in agreement with a previous result by Borovsky [1998], concluding that the major

408 factor determining the severity of that storm was the enhanced plasma sheet density. As

409 the large decrease on the *Dst* index (-100 nT) takes place between 16 UT and 17 UT

410 when the density increases sharply, we conclude that the interaction between the two

411 segments of the filament with opposite chilarities are the cause of the large variation on

412 the *Dst* for this event.

4. Summary and Conclusions

In this paper we have searched for the solar sources and related interplanetary structures that could have been associated with the seven largest *Dst* index decreases (*dDst/dt* ≤ -100 nT/hour) that took place along solar cycle 23. Such large and fast *dDst/dt* should have important role in triggering large GIC events, as discussed in the introduction.

M or X class flares were always involved in the solar sources that caused the large disturbance at terrestrial surface. Also at least one full halo CME, with a speed on the plane of sky above 900 km/s participated in every studied event, and two or more successive full or partial halo CMEs were involved in five out of the seven events. An increase in the event geoeffectiveness associated with successive halo CMEs has been proposed by Gopalswamy [2007], considering as indicator the minimum value reached by *Dst* as an indicator. Our results do seem to support such a proposal.

Concerning the interplanetary medium signatures, all events present a large southern B_z component, ranging between -37 nT and -77 nT. This high value takes place near or at a sheath/MC interface and is frequently associated with shock compression. The intensification in the $-B_z$ field can also be associated with a complex interaction/ compression between consecutive CMEs, as demonstrated by Wang et al. [2005], Lugaz et al. [2005, 2007] or Wu et al. [2002], which carried out MHD simulations of the interaction of two CMEs in the heliosphere. Both simulations reach different scenarios,. The simulation by Wu et al. [2002] obtains a cannibalization between CMEs due to magnetic reconnection near the Sun, where two CMEs merge, as might have occurred in event #7, with just one MC appearing in the interplanetary data. On the other hand, Wang et al. [2005] and Lugaz et al. [2005] present a double-MC formation (e.g. event #4) due the interaction taking place in the interplanetary medium, where the process of

438   merging becomes very slow due to the larger scale lengths and lower densities relative

439   to the proximities of the Sun. However, not only interactions between successive CMEs

440   but also the encounter between a high speed stream and a CME could also compress B_z

441   and enhance the event geoeffectiveness. Such interaction of MCs and high-speed

442   streams was addressed by Dal Lago et al. [2001] for three magnetic clouds. Event #3

443   could be related to this latter scenario.

444   Interaction between segments of a filament at the solar surface could be the

445   cause of an unusual high solar wind density and temperature inside a smooth magnetic

446   field observed for the event on November 20, 2003 (event #7). Large density and

447   temperature enhancements in the sheath could have triggered the large $dDst/dt$ for the

448   event on September 17, 2000, but in this case the interaction appears in the form of an

449   ejecta instead of a smooth magnetic field of a MC. In the other cases, successive MCs

450   appear at the interplanetary medium interacting between them, such as the events of

451   May 15, 2005 and March 31, 2001. In the events of November 6, 2001 and July 14,

452   2000, shocks appear to play a major role overtaking or compressing ICMEs. However,

453   this type of interaction is not exclusive of CMEs or their driven shock waves. During

454   the event on August 24, 2005 an MC is caught between two streams triggering the large

455   decrease in Dst index.

456   Although not analyzed in this paper due to a lower $dDst/dt$ threshold, the event

457   on January 21, 2005 already mentioned above, is also an interesting event similar to

458   those discussed above although the storm is not so intense (Dst_{peak} -105 nT). As

459   indicated by Du et al. [2008], an unusual double-discontinuity characterized by a non-

460   compressive density enhancement, together with an increase in the southward IMF in

461   the solar wind following the discontinuity led to the initial growth of the main phase of

462   this storm. Then, a large $dDst/dt$ decrease took place during northward IMF, together

463 with a large enhancement in the solar wind density as a result of the interaction between

464 the MC structure and the stream seen in interplanetary data. Such large density

465 enhancement could have played a key role in the large *Dst* decrease, as in the event on

466 August 24, 2005.

467 From the discussed possible solar/interplanetary causes of the large and fast *Dst*

468 decreases observed in the seven events of this paper, as listed on column 7 of Table 1,

469 one practically common feature was the presence of a compression process occurring at

470 the sheath field region of ICMEs due to one or more subsequent magnetic clouds

471 leading to an interesting and very geoeffective interface/discontinuity that deserves a

472 closer future study.

473 A systematic study using SYM-H index will also follow in the near future in order to

474 get light about how the temporal resolution used to compute the time derivative of the magnetic

475 field horizontal component (that is, hourly resolution limited by using *Dst* data) might impact

476 the study.

477

486   and plasma data from OMNIweb database, and *Dst* index from World Data Center for

487   Geomagnetism.

488

References

Belov, A. V., Gaidash, S. P., Eroshenko, E. A., Lobkov, S. L., Pirjola, R., and Trichtchenko, L. (2007): Effects of strong geomagnetic storms on Northern railways in Russia, *Proceedings of the 7-th International Symposium on Electromagnetic Compatibility and Electromagnetic Ecology*, Saint-Petersburg, Russia, 26–29 June 2007, 280–282.

Borovsky, J. (1998), Lightning energetics: Estimates of energy dissipation in channels, channel radii, and channel-heating risetimes, *J. Geophys. Res.*, 103(D10), 11537-11553.

Burlaga, L. (1974), Interplanetary Stream Interfaces, *J. Geophys. Res.*, 79(25), 3717-3725.

Burlaga, L. F., E. Sittler, F. Mariani, and R. Schwenn (1981), Magnetic loop behind an interplanetary shock: Voyager, Helios, and IMP 8 bservations, *J. Geophys. Res.,* 86, 6673–6684.

Burlaga, L. F., R. M. Skoug, C. W. Smith, D. F. Webb, T. H. Zurbuchen, and A. Reinard (2001), Fast ejecta during the ascending phase of solar cycle 23: Ace observations, 1998–1999, J. Geophys. Res., 106(A10), 20957–20977.

Burlaga, L. F., S. P. Plunkett, and O. C. St. Cyr (2002), Successive CMEs and complex ejecta, *J. Geophys. Res.*, 107(A10), 1266, doi:10.1029/2001JA000255.

Cid, C., E. Saiz, and Y. Cerrato (2008), Comment on "Interplanetary conditions leading to superintense geomagnetic storms (Dst ≤ −250 nT) during solar cycle 23" by E. Echer et al., Geophys. Res. Lett., 35, L21107, doi:10.1029/2008GL034731.

511   Cid, C., M. A. Hidalgo, E. Saiz, Y. Cerrato, and J. Sequeiros (2004), Sources of intense

512   geomagnetic storms over the rise of solar cycle 23, Solar Phys., 223, 231–243.

513   Chandra, R., Pariat, E., Schmieder, B., Mandrini, C., and Uddin, W. (2009), How can a

514   Negative Magnetic Helicity Active Region Generate a Positive Helicity Magnetic

515   Cloud?, *Solar Phys.*, 261(1), 26, 127-148.

516   Dal Lago, A., W.D. Gonzalez, A.L.C. de Gonzalez, and L.E.A. Vieira (2001),

517   Compression of magnetic clouds in interplanetary space and increase in their

518   geoefectiveness, J. Atmosph. Solar-Terr. Phys., 63, 451–455.

519   Dasso, S., et al. (2009), Linking two consecutive nonmerging magnetic clouds with

520   their solar sources, J. Geophys. Res., 114, A02109, doi:10.1029/2008JA013102.

521   Du, A. M., B. T. Tsurutani, and W. Sun (2008), Anomalous geomagnetic storm of 21–

522   22 January 2005: A storm main phase during northward IMFs, *J. Geophys. Res.*, 113,

523   A10214, doi:10.1029/2008JA013284.

524   Echer, E., W. D. Gonzalez, and B. T. Tsurutani (2008a), Interplanetary conditions

525   leading to superintense geomagnetic storms (Dst $\leq$ −250 nT) during solar cycle 23,

526   Geophys. Res. Lett., 35, L06S03, doi:10.1029/2007GL031755.

527   Echer, E., W. D. Gonzalez, B. T. Tsurutani, and A. L. C. Gonzalez (2008b),

528   Interplanetary conditions causing intense geomagnetic storms (Dst $\leq$ −100 nT) during

529   solar   cycle   23   (1996–2006),   *J.   Geophys.   Res.*,   113,   A05221,

530   doi:10.1029/2007JA012744.

531   Eroshenko, E.A., A.V. Belov, D. Boteler, S.P. Gaidash, S.L. Lobkov, R. Pirjola and L.

532   Trichtchenko (2010), Effects of strong geomagnetic storms on Northern railways in

533   Russia, Advances in Space Research, 46, 9, 1102-1110, doi: 10.1016/j.asr.2010.05.017

534   Farrugia, C. J., V. K. Jordanova, M. F. Thomsen, G. Lu, S. W. H. Cowley, and K. W.

535   Ogilvie (2006), A two-ejecta event associated with a two-step geomagnetic storm, *J.*

536   *Geophys. Res.*, 111, A11104, doi:10.1029/2006JA011893.

537   Gonzalez, W. D., E. Echer, A. L. Clua-Gonzalez, and B. T. Tsurutani (2007),

538   Interplanetary origin of intense geomagnetic storms ($Dst < -100$ nT) during solar cycle

539   23, Geophys. Res. Lett., 34, L06101, doi:10.1029/2006GL028879.

540   Gonzalez, W.D., B.T. Tsurutani and A.L.C. Gonzalez (1999), Interplanetary origin of

541   geomagnetic storms, *Space Sci. Rev.,* 88, 529–562, doi:10.1023/A:1005160129098.

542   Gonzalez, W. D., A. L. C. de Gonzalez, A. Dal Lago, B. T. Tsurutani, J. K. Arballo, G.

543   K. Lakhina, B. Buti, C. M. Ho, and S.-T. Wu (1998), Magnetic cloud field intensities

544   and solar wind velocities, Geophys. Res. Lett., 25(7), 963-966.

545   Gonzalez, W. D., B. T. Tsurutani, P. S. McIntosh, and A. L. Clúa de Gonzalez (1996),

546   Coronal hole-active region-Current sheet (CHARCS) Association with intense

547   interplanetary and geomagnetic activity, Geophys. Res. Lett., 23(19), 2577–2580.

548   Gonzalez, W. D., J. A. Joselyn, Y. Kamide, H. W. Kroehl, G. Rostoker, B. T. Tsurutani,

549   and V. M. Vasyliunas (1994), What is a Geomagnetic Storm?, *J. Geophys. Res.*,

550   99(A4), 5771–5792.

551   Gopalswamy, N., S. Yashiro, and S. Akiyama (2007), Geoeffectiveness of halo coronal

552   mass ejections, *J. Geophys. Res.*, 112, A06112, doi:10.1029/2006JA012149.

553   Gopalswamy, N., S. Yashiro, G. Michalek, H. Xie, R. P. Lepping, and R. A. Howard

554   (2005), Solar source of the largest geomagnetic storm of cycle 23, *Geophys. Res. Lett.*,

555   32, L12S09, doi:10.1029/2004GL021639.

556   Gosling, J., J. Asbridge, S. Bame, and W. Feldman (1978), Solar Wind Stream

557   Interfaces, J. Geophys. Res., 83(A4), 1401-1412.

558   Huttunen, K. E. J. , R. Schwenn, V. Bothmer, and H. E. J. Koskinen (2005), Properties

559   and geoeffectiveness of magnetic clouds in the rising, maximum and early declining

560   phases of solar cycle 23, Ann. Geophys., 23, 625-641.

561   Koen, J., and Gaunt, C.T. (2002), Geomagnetically induced currents at mid-latitudes,

562   *Proceedings of the 27-th General Assembly of the International Union of Radio Science*,

563   Maastrich, the Netherlands, 17-24 August 2002, 1-4.

564   Lario, D., A. Aran, and R. B. Decker (2008), Major solar energetic particle events of

565   solar cycles 22 and 23: Intensities above the streaming limit, *Space Weather*, 6, S12001,

566   1-25, doi:10.1029/2008SW000403.

567   Lepping, R. P., J. A. Jones, and L. F. Burlaga (1990), Magnetic Field Structure of

568   Interplanetary Magnetic Clouds at 1 AU, *J. Geophys. Res.*, 95(A8), 11957–11965,

569   doi:10.1029/JA095iA08p11957.

570   Lugaz, N., W. B. Manchester IV, I. I. Roussev, G. Tóth, and T. I. Gombosi (2007),

571   Numerical investigation of the homologous coronal mass ejection events from active

572   region 9236, ApJ., 659 788-800 doi: 10.1086/512005.

573   Lugaz, N., W. B. Manchester IV, and T. I. Gombosi (2005), Numerical simulation of

574   the interaction of two coronal mass ejections from Sun to Earth, *ApJ.*, 634, 651-662,

575   doi: 10.1086/491782.

576   Möstl, C., C. Miklenic, C. J. Farrugia, M. Temmer, A. Veronig, A. B. Galvin, B.

577   Vršnak, and H. K. Biernat (2008), Two-spacecraft reconstruction of a magnetic cloud

578   and comparison to its solar source, Ann. Geophys., 26, 3139–3152.

579   Saiz, E., C. Cid, Y. Cerrato (2008), Forecasting Intense Geomagnetic Activity using

580   Interplanetary Magnetic Field Data, *Ann. Geophys.*, 26, 3989-3998.

581   Richardson I. G., and J. Zhang (2008), Multiple-step geomagnetic storms and their

582   interplanetary drivers, *Geophys. Res. Lett.*, 35, L06S07, doi:10.1029/2007GL032025.

583   Rouillard, A. P., et al. (2009), A solar storm observed from the Sun to Venus using the

584   STEREO, Venus Express, and MESSENGER spacecraft, J. Geophys. Res., 114,

585   A07106, doi:10.1029/2008JA014034.

586   Smith et al. (2001), Ace observations of the Bastille day 2000 interplanetary

587   disturbances, *Solar Phys.*, 204, Numbers 1-2, 227-252, doi: 10.1023/A:1014265108171.

588   Vodyannikov, V. V., G. I. Gordienko, S. A. Nechaev, O. I. Sokolova, S. Yu. Khomutov

589   and A. F. Yakovets (2006), Geomagnetically induced currents in power lines according

590   to data on geomagnetic variations, *Geomagnetism and Aeronomy*, 46, 6, 809-813, doi:

591   10.1134/S0016793206060168.

592   Wang, R. (2007), Large geomagnetic storms of extreme solar event periods in solar

593   cycle 23, *Advances in Space Research*, 40, 1835–1841.

594   Wang Y., H. Zheng, S. Wang and P. Ye (2005), MHD simulation of the formation and

595   propagation of multiple magnetic clouds in the heliosphere, *A&A*, 434, 309-316 doi:

596   10.1051/0004-6361:20041423.

597   Wang, Y. M., P. Z. Ye, S. Wang, and X. H. Xue (2003a), An interplanetary cause of

598   large geomagnetic storms: Fast forward shock overtaking preceding magnetic cloud,

599   Geophys. Res. Lett., 30(13), 1700, doi:10.1029/2002GL016861.

Wang, Y. M., P. Z. Ye, and S. Wang (2003b), Multiple magnetic clouds: Several examples during March–April 2001, *J. Geophys. Res.*, 108 (A10), 1370, doi:10.1029/2003JA009850.

Wu, S. T., A. H. Wang, N. Gopalswamy (2002), MHD modelling of CME and CME interactions in a bi-modal solar wind: a preliminary analysis of the 20 January 2001 two CMEs interaction event, In: *SOLMAG 2002. Proceedings of the Magnetic Coupling of the Solar Atmosphere Euroconference and IAU Colloquium* 188, 11 - 15 June 2002, Santorini, Greece. Ed. H. Sawaya-Lacoste. ESA SP-505. Noordwijk, Netherlands: ESA Publications Division, ISBN 92-9092-815-8, 2002, 227–230.

Xie, H., N. Gopalswamy, P. K. Manoharan, A. Lara, S. Yashiro, and S. T. Lepri (2006), Long-lived geomagnetic storms and coronal mass ejections, *J. Geophys. Res.*, *111*, A01103, doi:10.1029/2005JA011287.

Xu, D., T. Chen, X.X. Zhang, and Z. Liu (2009), Statistical relationship between solar wind conditions and geomagnetic storms in 1998–2008, *Planet. Space Science,* 57, doi: 10.1016/j.pss.2009.07.015.

Yurchyshyn, V., C. Liu, V. Abramenko, and J. Krall (2006), The May 13, 2005 eruption: Observations, data analysis and interpretation, *Sol. Phys.*, *239*, 317–335, doi:10.1007/s11207-006-0177-3.

Zhang, J., et al. (2007), Solar and interplanetary sources of major geomagnetic storms ($Dst \leq -100$ nT) during 1996–2005, *J. Geophys. Res.*, *112*, A10102, doi:10.1029/2007JA012321.

621   Zhang, Y., W. Sun, X. S. Feng, C. S. Deehr, C. D. Fry, and M. Dryer (2008), Statistical

622   analysis of corotating interaction regions and their geoeffectiveness during solar cycle

623   23, *J. Geophys. Res.*, *113*, A08106, doi:10.1029/2008JA013095.

624 **Figure 1. Interplanetary data and *Dst* index measured for the event on May 15,**

625 **2005.** From top to bottom are plotted: magnetic field strength and GSM magnetic field

626 components, bulk speed, proton number density and radial component of the proton

627 temperature. The regions indicated by shadowed areas correspond to magnetic clouds,

628 as identified by Dasso et al. [2009]. The bottom panel shows the geomagnetic index

629 *Dst*. The shadowed area in this panel indicates the interval of the largest *dDst/dt* for this

630 event (see text for detail).

631 **Figure 2. Interplanetary data and *Dst* index measured for the event on November**

632 **6, 2001.** From top to bottom are plotted: magnetic field strength and GSM magnetic

633 field components, bulk speed, proton number density and radial component of the

634 proton temperature. Interplanetary data for this Figure comes from ACE Level 2

635 (verified) Data web site at http://www.srl.caltech.edu/ACE/ASC/level2/ in order to

636 avoid the data gap for magnetic field data for these dates at OMNIweb database.

637 Therefore, solar wind data are not shifted to the Earth Bow Shock Nose. The bottom

638 panel shows the geomagnetic index *Dst*. A first dashed-dotted line indicates the front

639 boundary of a magnetic cloud. An arrow indicates the region of the cloud, which rear

640 boundary cannot be established due to the data gap in solar wind plasma parameters.

641 The dashed line with an "S" indicates the overtaking shock identified by Wang et al.

642 [2003a].

643 **Figure 3. Interplanetary data and Dst index measured for the event on August 24,**

644 **2005.** From top to bottom are plotted: magnetic field strength and GSM magnetic field

645 components, bulk speed, proton number density and radial component of the proton

646 temperature. The bottom panel shows the geomagnetic index *Dst*. Two regions are

647 indicated in panel 5th corresponding to a slow and a fast wind. A dashed line with an "S"

648 in top panels (solar wind measurements) indicates a shock and shadowed area in these

649 panels corresponds to an ICME (see text for detail). The shadowed area in bottom panel

650 indicates the largest decrease in *Dst* index for the event.

651 **Figure 4. SOHO EIT images in the Fe XV band pass (284 Å).** A coronal hole close

652 to central meridian appears in the images. The ejection of the halo CME on August 22

653 at 01:31 UT took place from S11W54 between both images. The extension of the

654 coronal hole close to the central solar meridian (marked with a square) increases from

655 the first image to the second one.

656 **Figure 5. Interplanetary data and Dst index measured for the event on March 31,**

657 **2001.** From top to bottom are plotted: magnetic field strength and GSM magnetic field

658 components, bulk speed, proton number density and radial component of the proton

659 temperature. The bottom panel shows the geomagnetic index *Dst*. The regions indicated

660 by shadowed areas correspond to magnetic clouds, as identified by Wang et al. [2003b].

661 **Figure 6. Interplanetary data and Dst index measured for the event on July 14,**

662 **2000.** From top to bottom are plotted: magnetic field strength and GSM magnetic field

663 components, bulk speed, proton number density and radial component of the proton

664 temperature. The bottom panel shows the geomagnetic index *Dst*. Dashed lines with

665 "S1", "S2" and "S3" in top panels (solar wind measurements) indicate the three shocks

666 as indicated by Smith et al. [2001]. Gap at interplanetary data for this Figure cannot be

667 avoid by using Ace Level 2 (verified) Data, as also contain a data gap. The shadowed

668 area in bottom panel indicates the largest decrease in *Dst* index for the event.

669 **Figure 7. Interplanetary data and Dst index measured for the event on September**

670 **17, 2000.** From top to bottom are plotted: magnetic field strength and GSM magnetic

671 field components, bulk speed, proton number density and radial component of the

672 proton temperature. The bottom panel shows the geomagnetic index *Dst*. Two regions

673 are indicated with shadowed areas which correspond to a sub-cloud and an ejecta, inside

674 a Multi-MC region.

675 **Figure 8. Interplanetary data and *Dst* index measured for the event on November**

676 **20, 2003.** From top to bottom are plotted: magnetic field strength and GSM magnetic

677 field components, bulk speed, proton number density and radial component of the

678 proton temperature. Dashed line with an "S" indicates the fast forward shock driving the

679 magnetic cloud (wide shadowed area). The narrow dashed area corresponds to the

680 largest decrease in the *Dst* index.

681

682

Figure 1

683

684

Figure 2

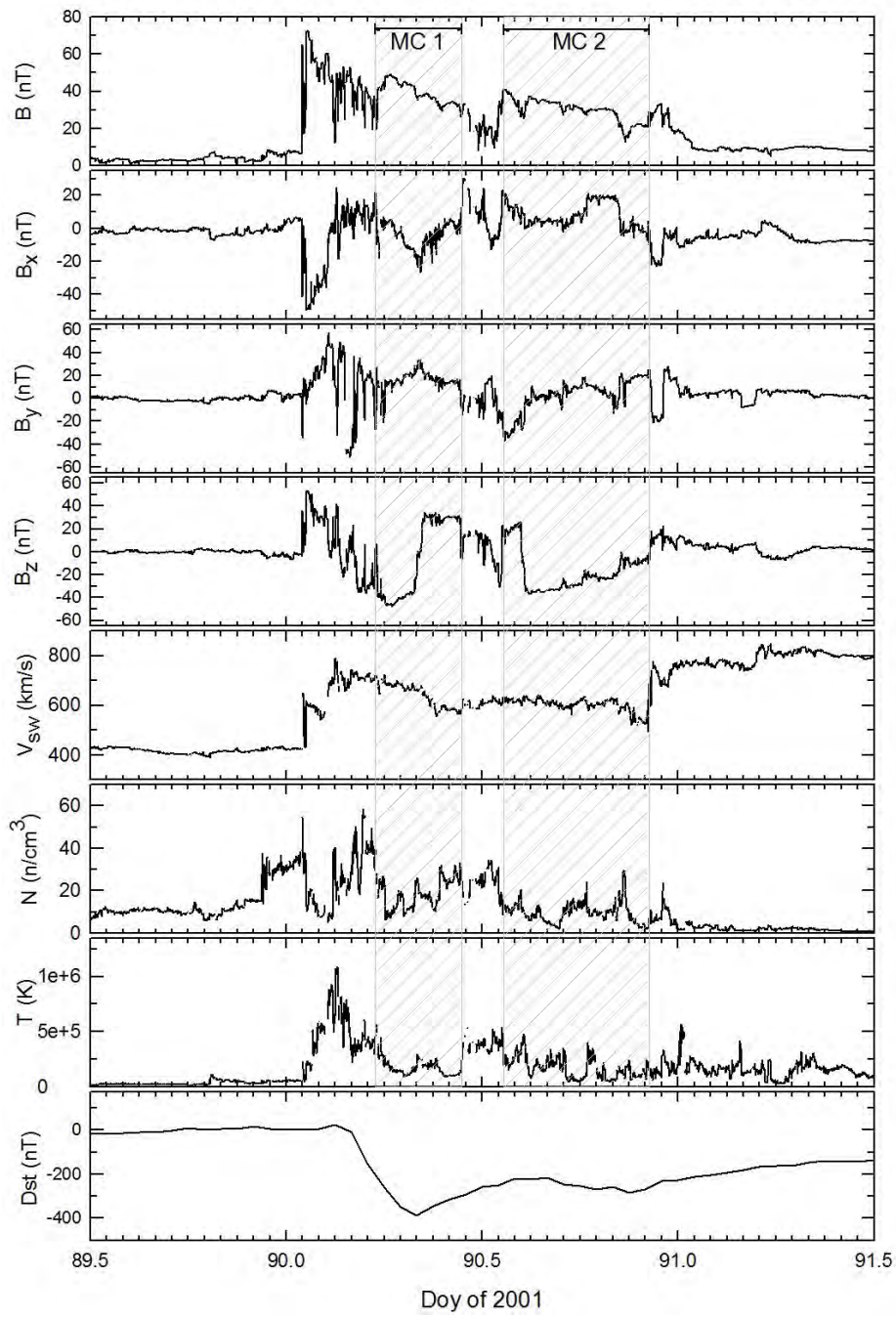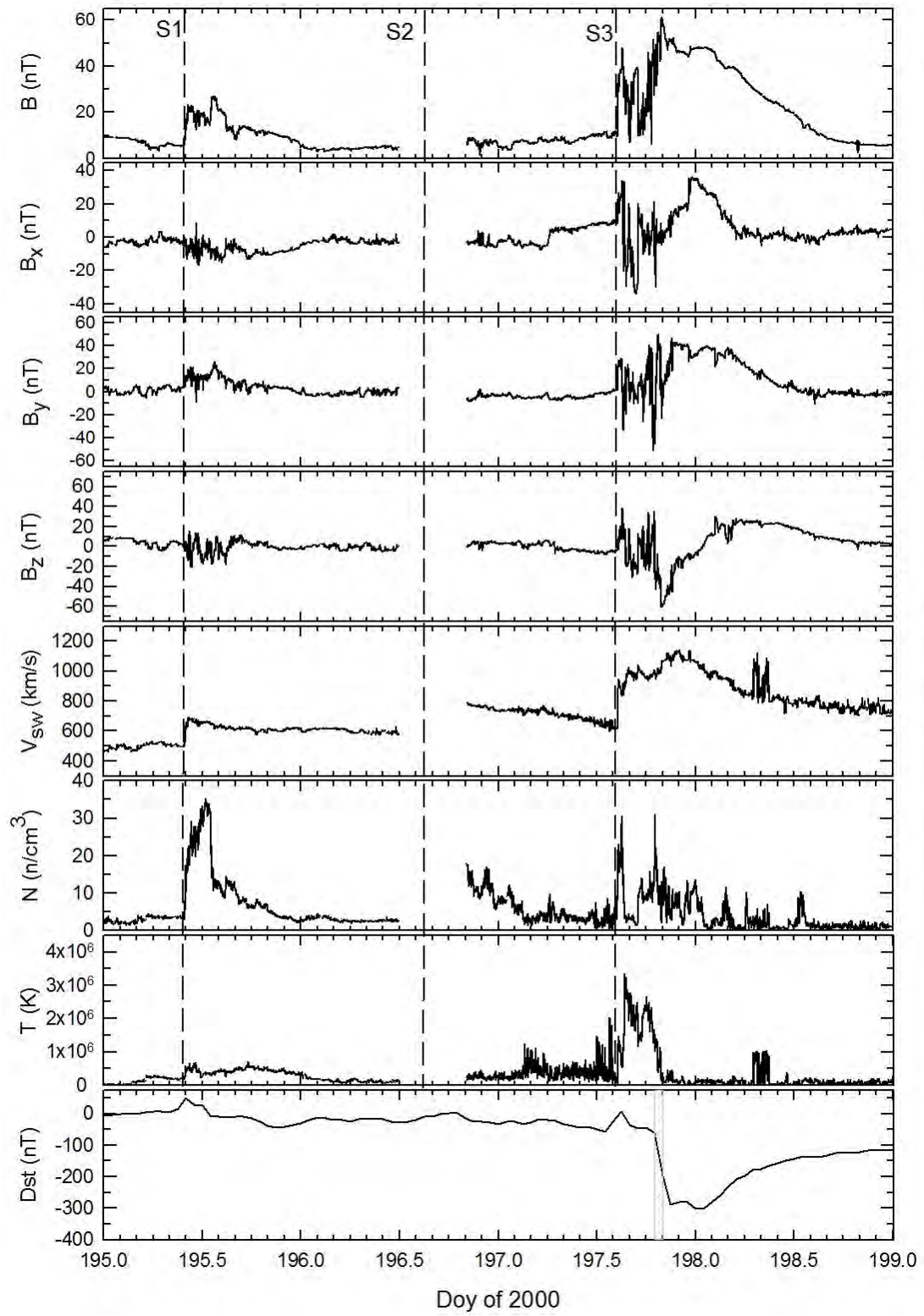Figure 3

Figure 4

690

691
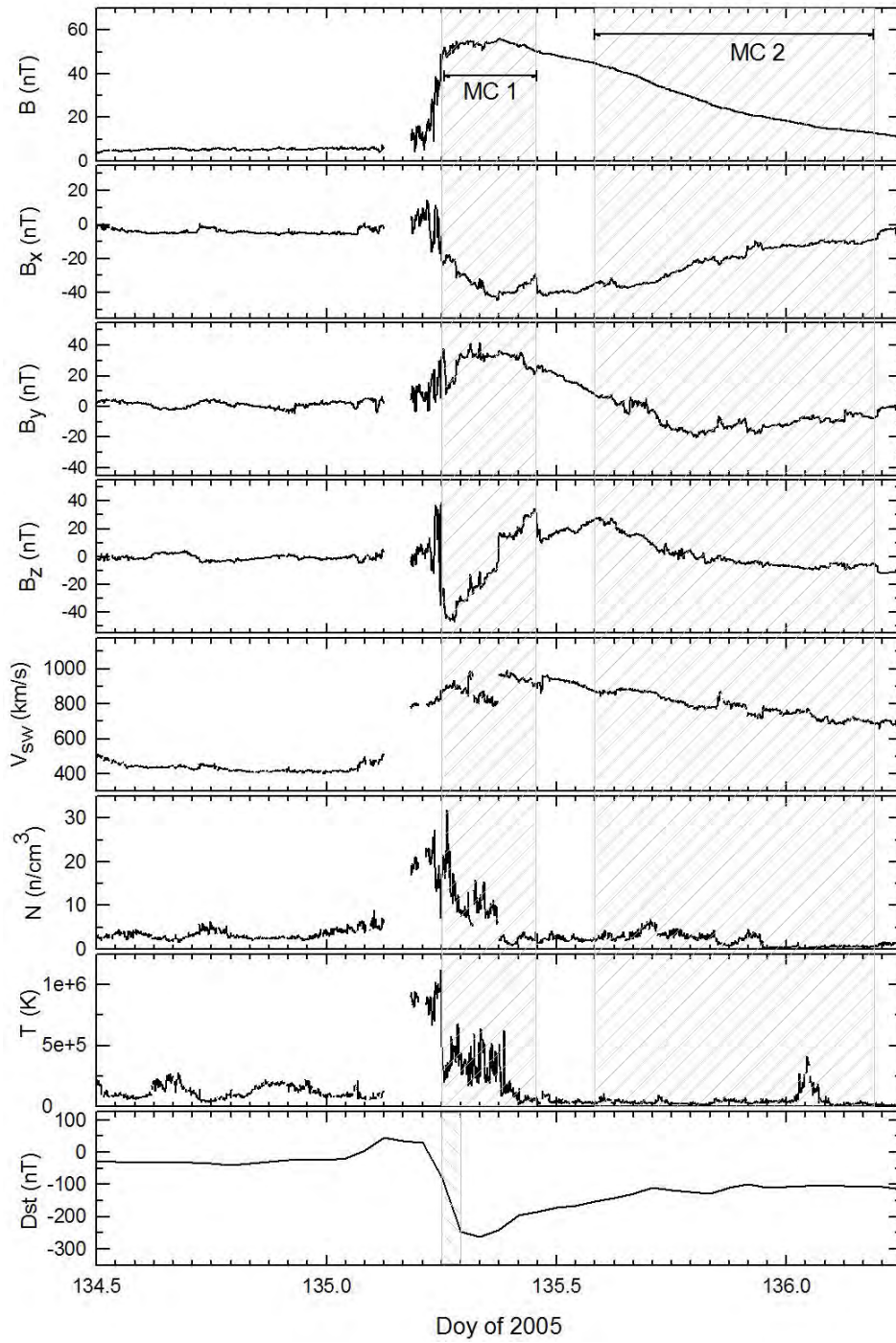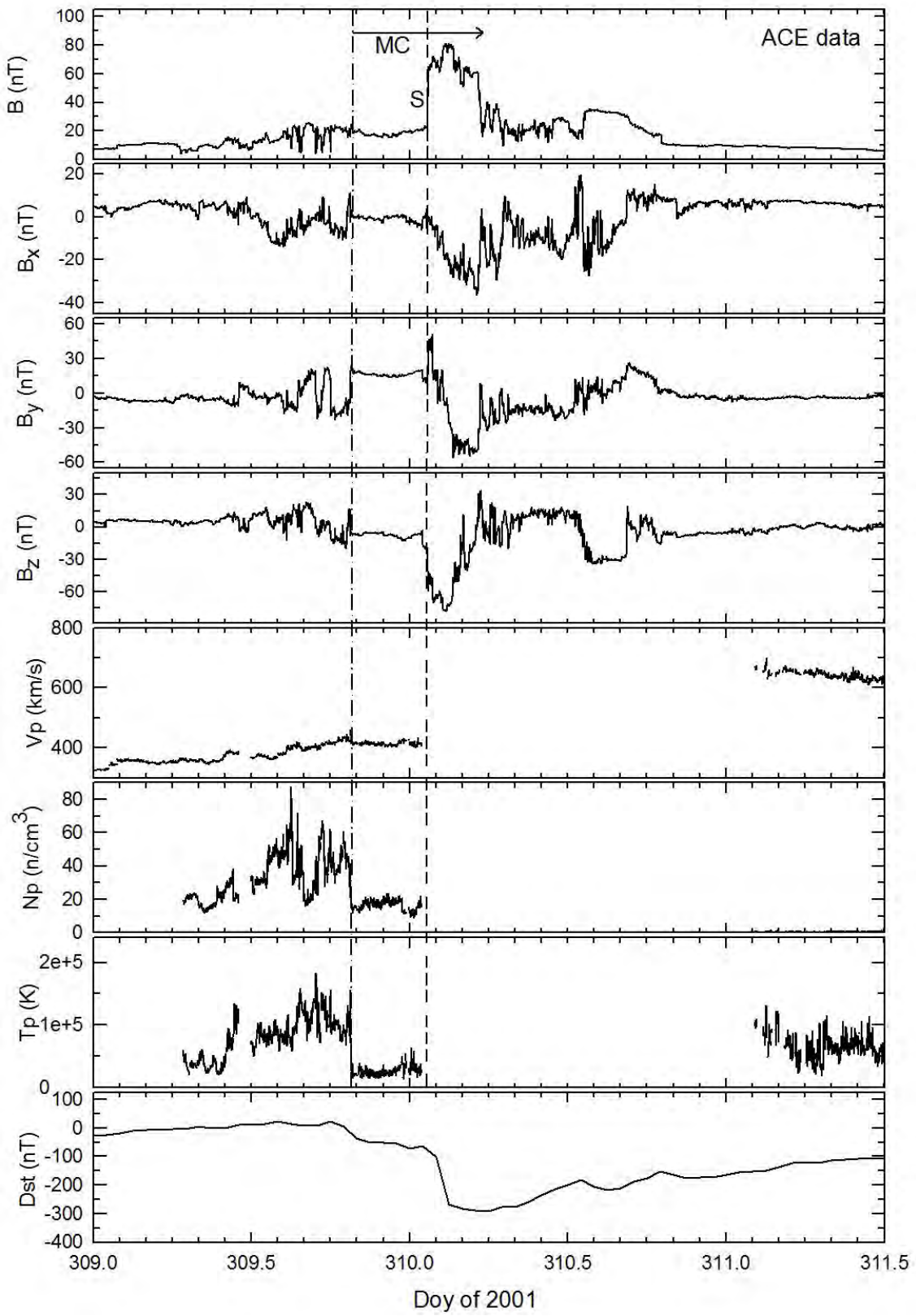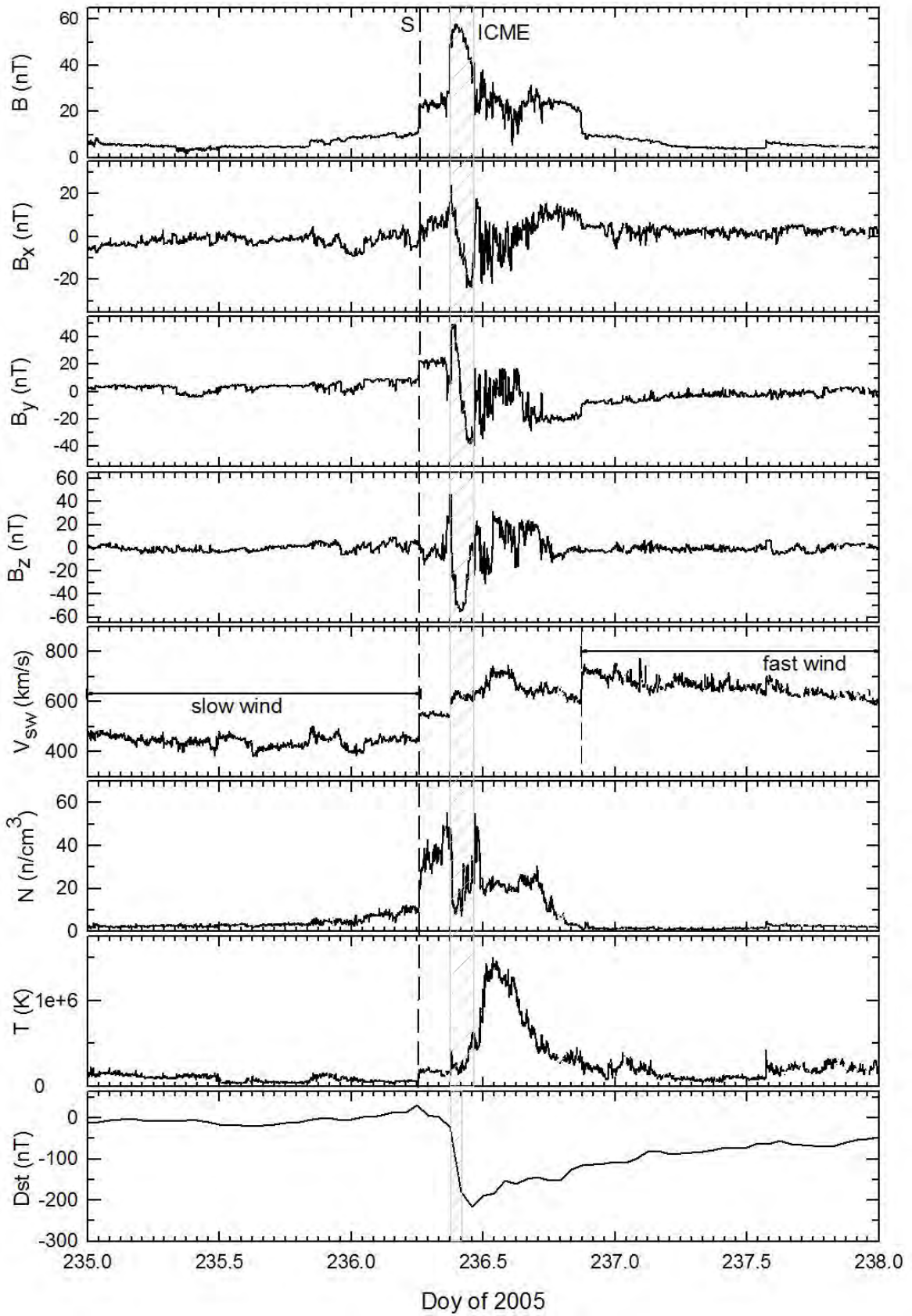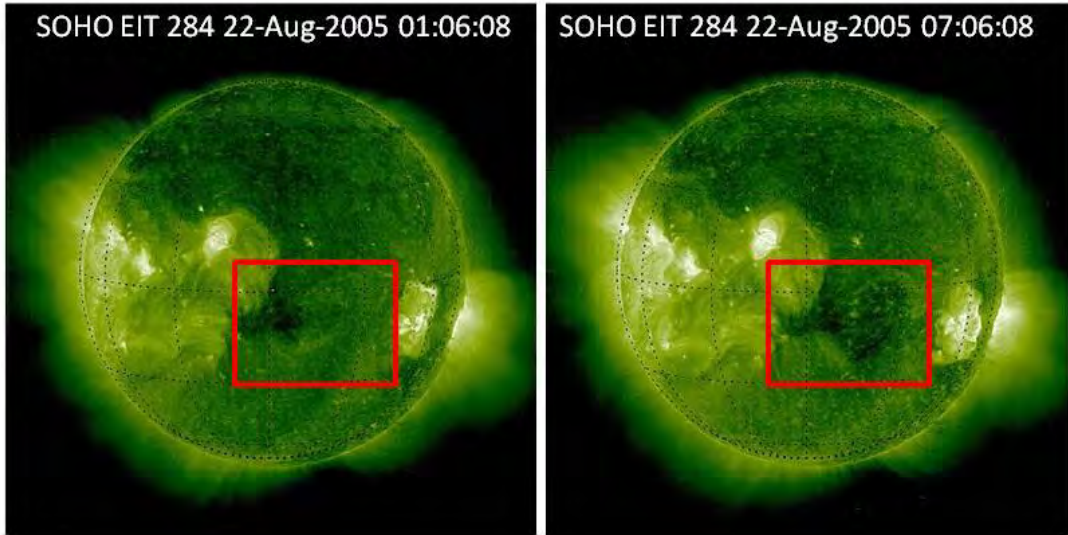
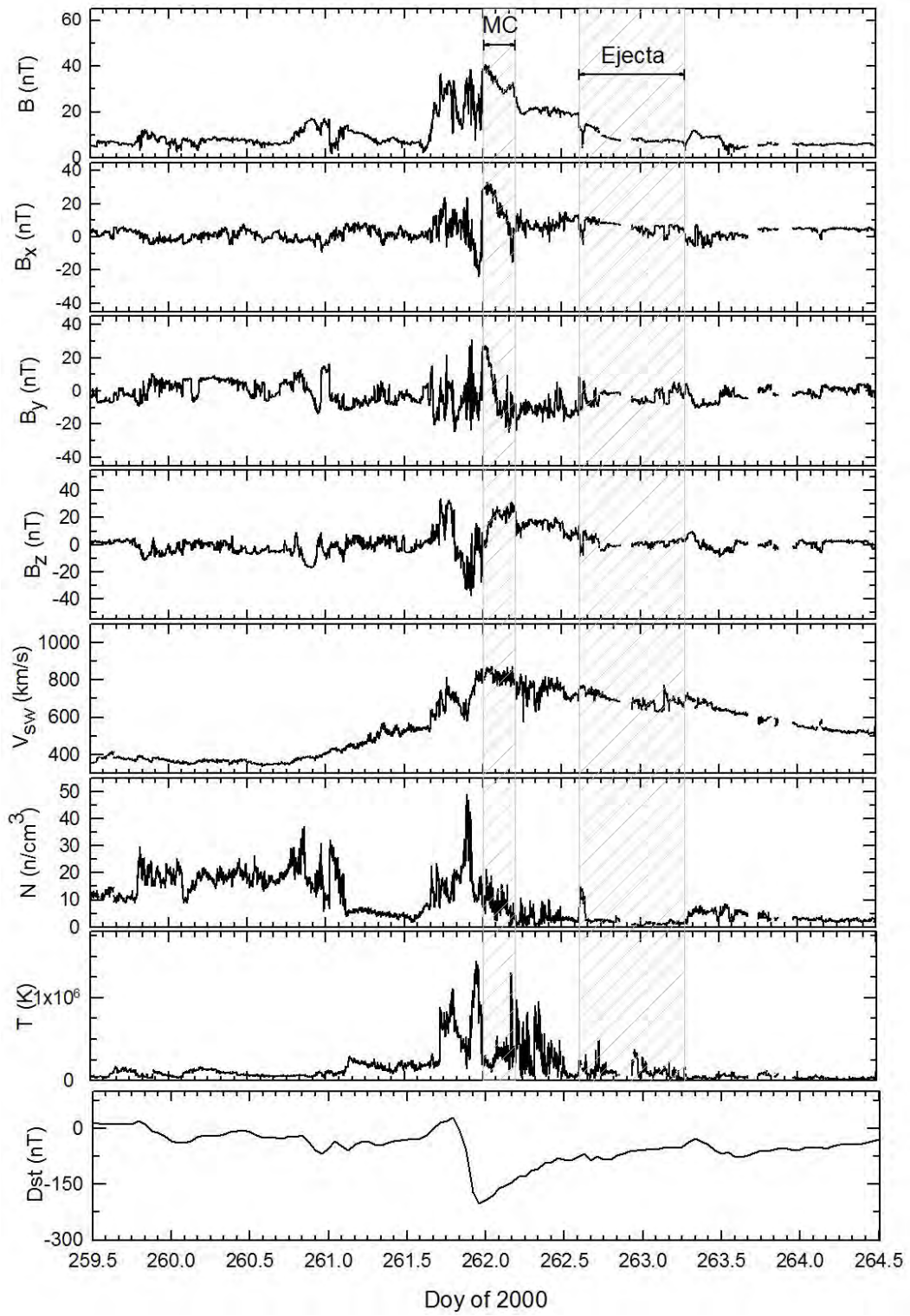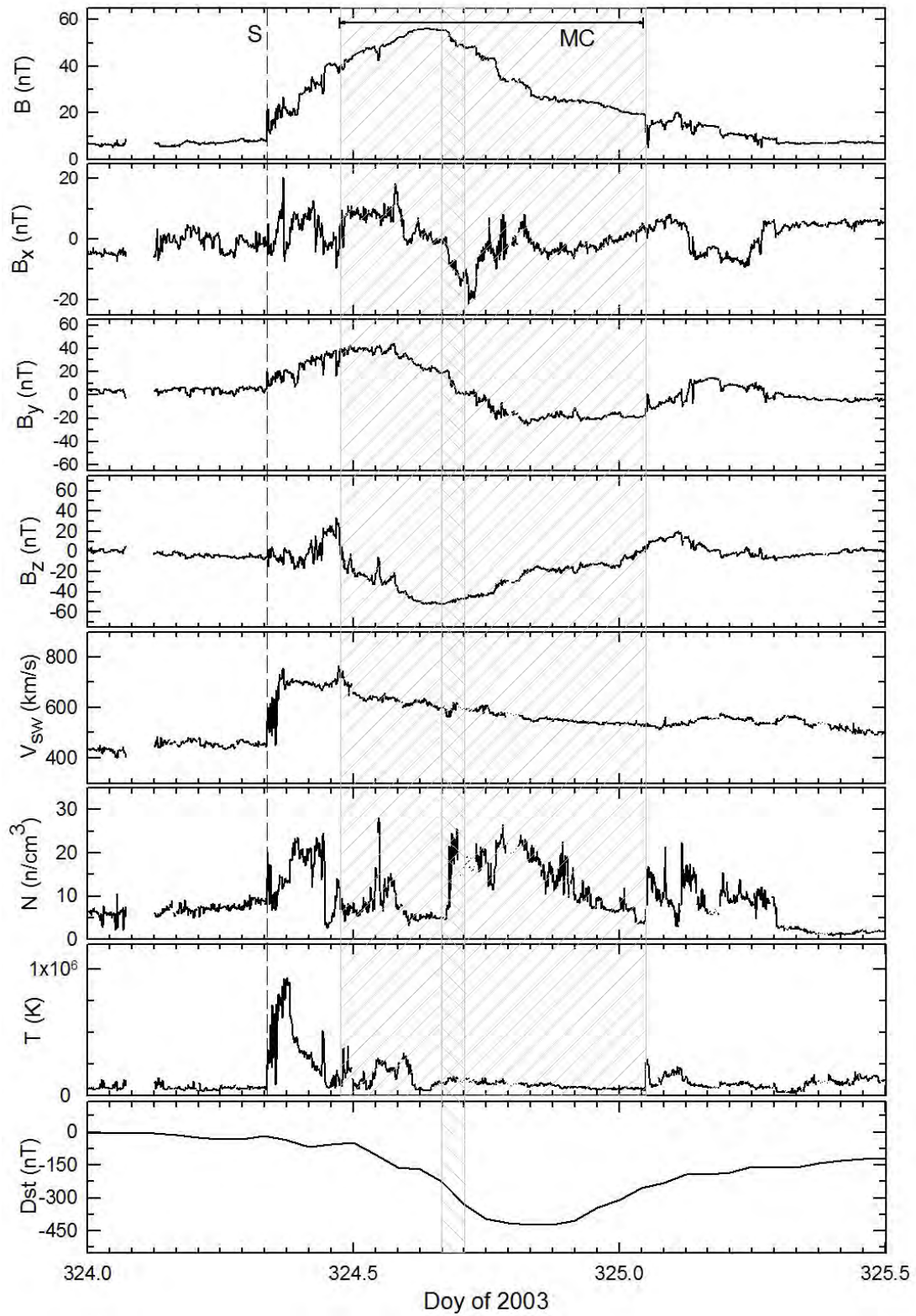Figure 5

Figure 6

Figure 7

Figure 8

Table 1. List of events of solar cycle 23 with $dDst/dt \leq$ -100 nT/hour arranged by the value of the $dDst/dt$, calculated as $Dst_{t+1hour}$ - Dst_t. The values in columns 2-5 (year, month, day, hour) corresponds to t. The minimum values reached in $dDst/dt$ and Dst, for every event, appear in columns 5 and 6, respectively. Column 7 shows interplanetary triggers for the large $dDst/dt$ events (see text for more details).

Event	$dDst/dt \leq$ -100 nT date				$(dDst/dt)_{min}$ (nT/hour)	Dst_{peak} (nT)	Trigger of $dDst/dt$
	yyyy	mm	dd	hh			
1	2005	05	15	06	-170	-263	Compressed MC by a second MC
2	2001	11	06	02	-168	-292	Overtaking shock through an ICME
3	2005	08	24	09	-158	-216	MC compressed by a fast stream
4	2001	03	31	04	-148	-387	Sheath and 1st MC of a Multi-MC
5	2000	07	15	19	-137	-301	Sheath compressed by succesive or merging of shock waves
6	2000	09	17	21	-110	-201	Sheath of a complex ejecta
7	2003	11	20	16	-100	-422	Possible interaction between segments of a filament